Diffusion of oxygen in Mg-doped α-Al$_2$O$_3$: the corundum conundrum explained

Andy Paul Chen,[1, *] W. M. C. Foulkes,[2] Arthur H. Heuer,[1, 3] and Michael W. Finnis[3, 2]

[1]*Department of Materials Science and Engineering,*
Case Western Reserve University, Cleveland, OH 44106-7204
[2]*Department of Physics, Imperial College, London SW7 2AZ*
[3]*Department of Materials, Imperial College, London SW7 2AZ*
(Dated: June 24, 2022)

It has been a puzzle for over two decades that the enhancement of oxygen diffusion in α-Al$_2$O$_3$, with respect to the amount of Mg doping, is several orders of magnitude *less* than expected. The standard model, which envisages that transport is mediated by oxygen vacancies induced to compensate the charge of Mg^{2+} ions substituting Al^{3+} ions, has not been able to explain this anomaly. Here, we report a detailed study of populations of point defects and defect clusters in Mg-doped α-Al$_2$O$_3$. By taking into account calculated defect formation energies from the literature, the condition of charge neutrality, and the environmental parameters (chemical potentials) under which the anomalous trend in oxygen diffusivities were previously observed, we are able to arrive at an explanation. A non-linear relationship between Mg concentration in the system and key native point defects, which serve as mediators of self-diffusion in α-Al$_2$O$_3$, is predicted: the concentrations of such defects increase much more slowly in the supersaturation regime than in the pre-saturation regime, matching the anomalous result previously observed in α-Al$_2$O$_3$. We identify the reason for this as buffering by positively charged Mg interstitials and Mg–oxygen vacancy clusters, which compensate the negative charges of Mg substitutional defects (Mg$_{\text{Al}}^{1-}$). This study answers part of the long-standing question about self-diffusion in alumina, referred to by Heuer and Lagerlöf in 1999 as the Corundum Conundrum.

I. INTRODUCTION

Defect-induced properties of aluminum oxide, in its stable phase corundum (α-Al$_2$O$_3$), have been extensively studied, because it is such a widely used ceramic. Some effects are visible to the naked eye. For example, while a relatively pure single crystal of α-Al$_2$O$_3$ is transparent, the introduction of transition metal ions generates various colors in the crystal depending on the element: Cr^{3+} ions produce the characteristic red hue of rubies, while a combination of Fe^{2+} and Ti^{4+} generates the hue of blue sapphire. In Ti-rich corundum, the precipitation of Ti defects to form oriented rutile (TiO$_2$) particles gives rise to the asterism in star sapphire [1].

The study of defects in α-Al$_2$O$_3$ has, however, been dogged by a puzzle known as the "Corundum Conundrum" since the term was coined by Heuer and Lagerlöf in 1999 [2], which has hitherto resisted attempts to resolve it [3–5]. The conundrum involves at its heart several points of disagreement between theoretical predictions and experimental observations. Chiefly among these is the observation that doping α-Al$_2$O$_3$ with MgO (TiO$_2$), to the point of saturation, increases (decreases) the oxygen diffusivity by a factor of ~ 100 (~ 50). In both cases that is orders of magnitude less than suggested by the simple theory in which charge compensating oxygen vacancies [6] would be the mobile species. It has been proposed that a yet-undiscovered buffering effect could be at play in the ensemble of defects, which replaces the expected charge-compensating defects [3, 4, 6].

Very recently, Futazuka *et al.*[7] performed a broad evaluation of defect formation energies in α-Al$_2$O$_3$ with impurities of group IIA (Be, Mg, Ca, Sr, Ba) and group IV (C, Si, Ge, Sn, Pb) elements using hybrid density functional theory (DFT) calculations, and identified dominant, native, charge-compensating defects corresponding to each impurity element at the specific temperatures $T = 300K$ and $T = 1800K$. In their study, a set of native (V_{Al}, V_{O}, Al$_i$, O$_i$, Al$_{\text{O}}$, and O$_{\text{Al}}$) and dopant-generated (X_{Al}, X_{O}, and X_i) point defects were included in the charge balance evaluations, although calculations of defect concentrations were not reported. In addition, defect pairs ([$V_{\text{Al}} \cdot V_{\text{O}}$] and [$X_{\text{Al}} \cdot V_{\text{O}}$]) were included in the set of defect species. It turns out that making use of their published formation energies, combined with appropriate experimental conditions, we can explain the conundrum for Mg-doped α-Al$_2$O$_3$ without involving any additional point defects or pairs, although for completeness we do test and reject a possible part played by [Mg$_{\text{Al}} \cdot$Al$_i$] pairs. A key requirement for this is our detailed analysis of the charged states and concentrations of the defects in equilibrium, with a self-consistent determination of the Fermi energy, and the experimental range of concentrations of dissolved Mg.

II. METHODOLOGY

A. Defect Formation Energy

The defect formation energy $\Delta E_f(T)$ is defined as the Gibbs energy needed to create one defect or defect cluster associated with a particular atomic site in the crys-

---

* andy.paul@u.nus.edu

tal, from reservoirs of defined chemical potential. This includes a reservoir of electrons if the defect is charged, in which case $\Delta E_f(T)$ is also a function of the Fermi energy, ε_F, besides the temperature T. We adopt here the common practice of neglecting the small vibrational contributions to these energies, which should be included in a more rigorous representation. For this reason the notation E rather than G is used. However, it should be emphasized that the most important temperature-dependant contribution to the Gibbs energy of formation of a defect comes from the chemical potential of the atoms in the notional reservoir to or from which they are transferred in the process of formation. Considering that n_i atoms of species i, with chemical potential μ_i, are introduced (positive Δn_i) or removed (negative Δn_i) by the formation of a certain defect D^q (with charge q), ΔE_f can be determined through the Zhang-Northrup equation [7, 8]:

$$\Delta E_f(D^q) = E_T(D^q) - E_T^{\text{perf}} - \sum_i \Delta n_i \mu_i + q(\varepsilon_F), \quad (1)$$

where $E_T(D^q)$ is the total energy of the simulation cell containing defect (D^q), and E_T^{perf} is the total energy of the same simulation cell without the defect. For consistency with Futazuka's DFT studies [7], we use the HSE hybrid exchange-correlation functional and take the energy of the valence band maximum, ε_{VBM}, as the reference energy. The chemical potential terms μ_{Al} and μ_{O} are required to satisfy the equilibrium condition $2\mu_{\text{Al}} + 3\mu_{\text{O}} = E(\text{Al}_2\text{O}_3)$, where $E(\text{Al}_2\text{O}_3)$ is the total Gibbs energy per unit of Al_2O_3 in the crystal. The control parameter here, for a system in a gaseous environment, is usually the oxygen partial pressure, p_{O_2}, and over the usual range of pressure and temperature, the environmental oxygen is almost entirely in the form of O_2 molecules. The effective chemical potential of oxygen atoms, μ_{O}, is just half of the chemical potential per oxygen molecule, since there is a notional equilibrium between oxygen in diatomic and monatomic form. For computational purposes, it is unnecessary to obtain these quantities entirely from theory, since an equation can be fitted to the experimental data describing the gas-phase heat capacity of oxygen [9] versus temperature, which accounts for the translational, vibrational and rotational contributions to the free energy of the molecules. A quadratic form in temperature was fitted to this data for O_2 at standard pressure, with an accuracy of better than 3 kJ/mol O_2 (20meV/atom) for temperatures up to 1800K:

$$\mu_{\text{O}}(\text{exp}) = \frac{1}{2}\left[\alpha T^2 + \beta T + \gamma + k_B T \ln\left(\frac{p_{\text{O}_2}}{p_{\text{O}_2}^{\circ}}\right)\right], \quad (2)$$

with the parameters $\alpha = -2.26 \times 10^{-7}\text{eV/K}^2$, $\beta = -2.05 \times 10^{-3}\text{eV/K}$, $\gamma = -0.0118\text{eV}$, and $p_{\text{O}_2}^{\circ} = 0.1$ MPa. The last term in (2) is added to the quadratic

form in order to describe the dependence of the chemical potential of oxygen on its partial pressure, referred to its standard state. This expression uses the standard reference states, which the chemistry community has designed to be compatible for all substances, whereby the enthalpy of all pure elements in their standard states at equilibrium is defined to be zero. Now, in order to combine it with DFT energies in (1), we need to shift the origin of chemical potential to the value that is implicit in our DFT calculations. It should be clear that such a shift for any element must be dependant on the choice of its pseudopotential, but this dependence cancels out in all measurable quantities. In this paper we have used the low-temperature formation energies calculated by Futazuka *et al.* [7], hence for consistency we have implicitly adopted their temperature-independent shift to the chemical potential of oxygen, which they refer to as $\frac{1}{2}E_{\text{O}_2}(T = 0, p_{\text{O}_2} = p_{\text{O}_2}^{\circ})$ (see eqn. (3) of ref. [7]).

B. Defect Concentrations

The concentration $[D^q]$ of a point defect or defect cluster in bulk Al_2O_3 is specified by ΔE_f, and the temperature, together with the concentration of sites N_s on which it can occur, and the multiplicity Ω of configurations at each site that the defect cluster can adopt in the crystal environment. N_s and Ω will enter as prefactors in the familiar Arrhenius relation in order to model the full configurational entropy in the dilute solution model. Since for simple point defects on lattice sites there are no orientational degrees of freedom, they can be neglected in elementary treatments of point defect concentrations. For more complex defects, such as a dumbbell interstitial, Ω also counts the possible orientations of the defect in the site having the same energy. For each species, this approach considers only the discrete configurations of equal energy, thus decoupling the vibrations of atoms from their hopping between sites and orientations. The result is the Boltzmann relation:

$$[D^q] = N_s \Omega \exp\left(-\frac{\Delta E_f}{k_B T}\right). \quad (3)$$

To determine defect concentrations at a particular temperature T, it is necessary to specify the value of ε_F. To this end, we proceed from the assumption of zero net charge in the bulk crystal; more precisely, the sum of charge contributions from all charged point defects or defect clusters, electrons in the conduction band (with concentration c_e), and holes in the valence band (with concentration c_h) is zero. Thus

$$-\sum_{D^q} q[D^q] + c_e - c_h = 0. \quad (4)$$

Fermi statistics dictate that the concentrations of electrons and holes can be expressed as functions of temper-

ature, Fermi energy, and the density of states, $\mathrm{DOS}(\varepsilon)$:

$$c_e = \int_{\varepsilon_{\mathrm{CBM}}}^{\infty} \mathrm{DOS}(\varepsilon) \cdot \frac{1}{1 + \exp\left(\frac{\varepsilon - \varepsilon_F}{k_B T}\right)} d\varepsilon, \mathrm{and} \quad (5)$$

$$c_h = \int_{-\infty}^{\varepsilon_{\mathrm{VBM}}} \mathrm{DOS}(\varepsilon) \cdot \left(1 - \frac{1}{1 + \exp\left(\frac{\varepsilon - \varepsilon_F}{k_B T}\right)}\right) d\varepsilon. \quad (6)$$

Since the electron and hole concentrations are monotonic in ε_F, we can easily find a unique solution for ε_F for which the charge neutrality condition of Equation 4 is satisfied. This solution is derived through an iterative minimization of the magnitude of the total charge in the system, arriving at the value of the Fermi energy (accurate to $\pm 0.2 \times 10^{-7}\mathrm{eV}$) which satisfies Equation 4. The concentrations of individual point defects, point-defect pairs, electrons and holes can then be derived using Equations 3, 5, and 6.
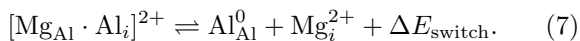
C. Bound Pairs of Point Defects

As Equation 4 assumes that the entire population of point defects and defect clusters is accounted for, it is desirable to find a set of defects that is as complete as possible. An exhaustive set of point defects can be trivially derived by listing all possible vacancies, antisite defects, interstitial defects, or substitutional defects with a dopant atom. However, an exhaustive set of defect clusters is unattainable, and assumptions are necessary to include the most reasonable defect cluster configurations in our calculations. We restrict our search to those constructed from a pair of point defects.

A useful construction principle is to consider oppositely charged defects that might be bound to each other by strong electrostatic forces; for instance, $\mathrm{Ti}_{\mathrm{Al}}^{1+}$ and V_{Al}^{3-} [10] would form the pair $[\mathrm{Ti}_{\mathrm{Al}} \cdot V_{\mathrm{Al}}]^{2-}$ and $\mathrm{Mg}_{\mathrm{Al}}^{1-}$ and V_{O}^{2+} would form the pair $[\mathrm{Mg}_{\mathrm{Al}} \cdot V_{\mathrm{Al}}]^{1+}$ [4].

It is also worth considering the two other defect pairs comprising an Mg-containing defect and a substitutional defect: $[\mathrm{Mg}_{\mathrm{Al}} \cdot \mathrm{Al}_{\mathrm{O}}]^q$ and $[\mathrm{Mg}_{\mathrm{Al}} \cdot \mathrm{Al}_i]^q$. From our results in Figures 1 and 2, we see that the energy of formation for antisite defects such as Al_{O} are so high as to make any cluster such as $[\mathrm{Mg}_{\mathrm{Al}} \cdot \mathrm{Al}_{\mathrm{O}}]^q$ very unlikely.

The case of $[\mathrm{Mg}_{\mathrm{Al}} \cdot \mathrm{Al}_i]^q$ is somewhat more complex, considering that Al_i^{3+} is relatively abundant in the system. However, we have verified as follows that a hypothetical bound pair of $\mathrm{Mg}_{\mathrm{Al}}^{1-}$ and Al_i^{3+} should collapse into a simple point defect Mg_i^{2+} by switching the positions of the substitutional Mg and interstitial Al:

$$[\mathrm{Mg}_{\mathrm{Al}} \cdot \mathrm{Al}_i]^{2+} \rightleftharpoons \mathrm{Al}_{\mathrm{Al}}^0 + \mathrm{Mg}_i^{2+} + \Delta E_{\mathrm{switch}}. \quad (7)$$

Structural optimization and total-energy calculations are performed in the DFT framework with the Vienna Ab-initio Simulation Package (VASP) [11–14], using a rhombohedral supercell containing $3 \times 3 \times 3$ primitive α-$\mathrm{Al}_2\mathrm{O}_3$ cells. The total energies of the supercell containing $[\mathrm{Mg}_{\mathrm{Al}} \cdot \mathrm{Al}_i]^{2+}$ or a point defect Mg_i^{2+} are compared. $2 \times 2 \times 2$ k-points are used in the sampling of the first Brillouin zone in the reciprocal space, corresponding to a k-point spacing of $0.032\,\text{Å}^{-1}$. PBE functionals are used to represent the atomic species Al, oxygen, and Mg. Our result shows the collapse reaction in Equation 7 to be spontaneous, with the energy output $\Delta E_{\mathrm{switch}}$ on the order of 2.4 eV. The omission of the defect pair $[\mathrm{Mg}_{\mathrm{Al}} \cdot \mathrm{Al}_i]^q$ is thus justified in our evaluation of the charge balance and defect chemistry of the system.

D. Density of states of α-$\mathrm{Al}_2\mathrm{O}_3$

Given the importance of the Fermi energy ε_F in predicting defect concentrations via defect formation energies ΔE_f, it follows that an accurate model of the band structure and DOS is required in order to generate ε_F self-consistently with the equations in Section II B. While standard DFT methods are adequate for structure prediction, they underestimate band gaps, which would be a problem for the determination of electron and hole densities. We address this source of error *post hoc* by using a hybrid functional to recalculate the electronic structure from the atomic positions. The density of states function $\mathrm{DOS}(\varepsilon)$ is calculated based on the settings adopted by Futazuka *et al.* [7] for consistency: To start with, the primitive trigonal unit cell of α-$\mathrm{Al}_2\mathrm{O}_3$ is used as the simulation cell. Structural optimizations are first performed with VASP, on a primitive unit cell of α-$\mathrm{Al}_2\mathrm{O}_3$ using the local density approximation (LDA) functional [15]. The convergence criterion for iterative structural optimization loops is reached when the forces on all the atoms fall below $0.05\,\mathrm{eV/Å}$, while electronic convergence is achieved when the energy change between successive electronic steps falls below 1 meV. The resultant α-$\mathrm{Al}_2\mathrm{O}_3$ unit cell has the lattice parameters $a = b = c = 5.095\,\text{Å}$ and $\alpha = \beta = \gamma = 55.29°$. In comparison, the corresponding experimental parameters are $a = b = c = 5.129\,\text{Å}$ and $\alpha = \beta = \gamma = 55.29°$ [16]. Structural relaxation with the LDA functional underestimates the cell volume by $\sim 2\%$, similar to previous calculations (e.g. [17]), and produces a much better agreement than generalized gradient approximation (GGA) [18, 19] or Perdew-Burke-Ernzerhof (PBE) [20, 21] functionals, which overestimate the cell volume by $\sim 5\%$.

Next, the Heyd-Scuseria-Ernzerhof (HSE) hybrid functional with the standard preset screening parameter $0.20\,\text{Å}^{-1}$ is adopted. As in Futazuka *et al.* [7], the proportion of the HSE functional represented by the Hartree-Fock equation is set to 40% to replicate the experimental band gap of 9.1eV [22, 23]; Partial occupancies are treated by Gaussian smearing, with the smearing width $\sigma = 0.1\mathrm{eV}$. For both steps, a Monkhorst-Pack mesh of $7 \times 7 \times 7$ k-points is used to sample the reciprocal space,

maintaining the k-point spacing at $\sim 0.028\,\mathring{A}^{-1}$.

E. Simulation with Experimental Conditions

In our evaluation of defect concentrations, although we can use the values of ground-state defect formation energies $\Delta E_f(D^q, \varepsilon_F = 0, T = 0K)$ of native and Mg-containing defects and defect clusters from Futazuka *et al.* [7], we still have to provide the dependence of ΔE_f on temperature, chemical potentials and Fermi energy (the chemical potential of electrons), in order to obtain results that correspond to the specific experimental conditions with which Lagerlöf, Mitchell, and Heuer [6] measured oxygen diffusion in doped α-Al$_2$O$_3$, namely $T = 1673.15K$ (1400°C) and $p_{O_2} = 0.21$ atm. We also need to calculate the concentration of Mg, and how it is distributed over the different types of defects. Futazuka *et al.* [7] defined μ_{Mg} according to the dominant secondary phase MgAl$_2$O$_4$: a solution for μ_{Mg} is attained through the constraints presented above and the equilibrium condition $2\mu_{Al} + 4\mu_O + \mu_{Mg} = E(MgAl_2O_4)$, where $E(MgAl_2O_4)$ is the total energy of each molecular unit of MgAl$_2$O$_4$. This value of μ_{Mg} (2.14 eV), hereafter denoted μ_{Mg}^0, corresponds to the solubility limit of Mg in α-Al$_2$O$_3$. However, as we shall see, the theoretical concentration of Mg in solution with this approach turns out to be much lower than in the experimental case (252 wt. ppm), which we have to suppose was supersaturated, since no precipitates were observed. In order to match the experimental data we found it necessary to adjust the theoretical concentration of Mg in solution, and to accomplish this we regard μ_{Mg} as the independent variable, and we control it by introducing the parameter A, such that $\mu_{Mg} = \mu_{Mg}^0 + A$. Our choices of μ_{Mg}, given in Table I, determine the Mg concentration, which we have calculated over the range from 10^{-12} to 252 wt. ppm.

It is prudent to note that only native defects and Mg-containing defects are factored into the defect concentration calculations, to the exclusion of any other aliovalent impurities (for example, Ti^{4+}) which may be present in experiment in smaller concentrations. However, our conclusions relate mainly to the high Mg-doping limit, where the concentration of Ti is minuscule compared to that of Mg (see Table I of Reference [6]), and would not be able to affect our results significantly.

III. RESULTS AND DISCUSSION

The defect formation energies as a function of Fermi energy, ε_F, evaluated at the experimental temperature $T = 1400$°C, ambient oxygen $p_{O_2} = 0.21$ atm, and experimental Mg concentration, 252 wt. ppm, are presented in Figure 1(a). Both the Mg content and the p_{O_2} affect the ε_F, and all three parameters determine the defect concentrations. Following our self-consistent calculations of the equilibrium defect concentrations, to be discussed below,

TABLE I. The modulated Mg chemical potentials μ_{Mg} and Fermi energies $\Delta\varepsilon_F = \varepsilon_F - \varepsilon_{VBM}$ (both in eV) for various Mg concentrations used in this study. Here, the case $\mu_{Mg} = 2.14$ eV corresponds to the solubility limit of Mg in Al$_2$O$_3$. The temperature and pressure of the system are set to the experimental values of $T = 1673.15K$ (1400°C) and $p_{O_2} = 0.21$ atm following Ref. [6]. The Fermi energy of the un-doped α-Al$_2$O$_3$ is included for reference.

Ambient			Reductive Limit		
μ_{Mg}	Mg (wt. ppm)	$\Delta\varepsilon_F$	μ_{Mg}	Mg (wt. ppm)	$\Delta\varepsilon_F$
2.95	252	2.71	2.95	252	4.52
2.54	16	2.73	2.64	16	4.55
2.14	1.4	2.82	2.14	2.14	4.72
1.64	0.11	2.96	1.64	0.38	4.96
1.14	0.010	3.11	1.14	0.067	5.20
0.72	0.0014	3.25	0.64	0.012	5.45
0.29	1.9×10^{-4}	3.39	0.14	0.0020	5.70
-0.14	2.6×10^{-5}	3.53	-0.36	1.2×10^{-4}	5.79
-0.56	3.3×10^{-6}	3.65	-0.76	7.6×10^{-6}	5.79
-1.15	6.8×10^{-8}	3.69	-1.26	2.4×10^{-7}	5.80
-1.74	1.1×10^{-9}	3.69	-1.86	3.7×10^{-9}	5.80
-2.26	3.1×10^{-11}	3.69	-2.46	5.7×10^{-11}	5.80
-2.76	9.7×10^{-13}	3.69	-3.03	1.1×10^{-12}	5.80
—	0	3.69	—	0	5.80

we have marked on Figure 1 the resulting Fermi energies, both with and without Mg doping, by dashed and solid vertical lines, respectively. For un-doped α-Al$_2$O$_3$, the Fermi energy lies at 3.69 eV in the ambient oxygen regime. For comparison purposes, Figure 1(b) shows how all the results in 1(b) would look if the p_{O_2} were reduced to the level at which the Al$_2$O$_3$ would be in equilibrium with metallic Al. In this case, all the formation energies and concentrations are changed and after calculation of the defect concentrations we find the Fermi level raised to 5.80 eV in un-doped Al$_2$O$_3$.

An increase in ε_F will naturally favor negatively charged defects, compared to those with positive charge. The slope of the formation energy of a defect versus ε_F is a direct measure of the charge on the defect, as shown graphically in Figure 1. Thus the formation energy of each defect, in its charge state of lowest-energy, is a piece-wise continuous and convex function of ε_F. With increasing ε_F, the slope of the formation energy decreases abruptly in increments of 1 for each newly acquired electron. Recalling that, in order to achieve equilibrium, the Fermi energy must adopt a value at which the total charge in the system is zero, the replacement of Al in the crystal by Mg reduces the Fermi energy, because an Al atom had donated three electrons to the valence band, but the Mg atom can only donate two. Note also the increase in Fermi energy under reducing conditions, which are most extreme in Figure 1(b). The explanation is straightforward. Removal of oxygen atoms from the lattice is obviously favoured by the low ambient p_{O_2}, which lowers the formation energy of oxygen vacancies. At the same time, given that the sum $2\mu_{Al} + 3\mu_O$ must
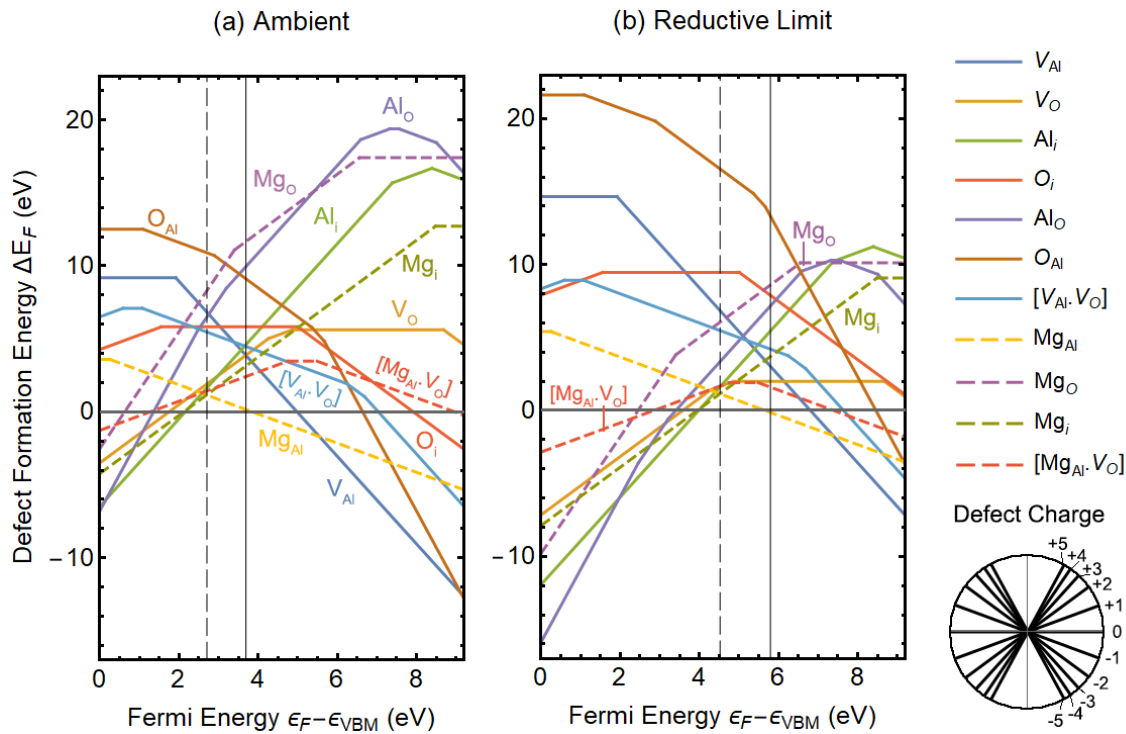
(a) Ambient **(b) Reductive Limit**

FIG. 1. Formation energies of native α-Al_2O_3 and Mg impurity defects, based on Ref. [7] and readjusted to the experimental temperature [6] of $T = 1673.15K$ (1400°C), and partial pressure of oxygen, $p_{O_2} = 0.21\,atm$ in (a) and, for comparison purposes, to the reductive limit in (b), which would correspond to equilibrium with metallic Al. Formation energies of Mg-containing defects are calculated using the chemical potential of Mg that was adjusted to give a total Mg content of 252 wt. ppm. The gradient of each linear segment in the defect formation energy corresponds to the dominant charge state of the defect at a given energy; a visual map relating charge state to gradient is included below the legend. The Fermi energy of the un-doped (Mg-doped) α-Al_2O_3 is marked by solid (dashed) vertical lines.

remain nearly constant and equal to the Gibbs energy per formula unit of the perfect crystal, the low p_{O_2} *raises* the formation energy of Al vacancies. Bearing in mind the constraint of total charge neutrality, if the p_{O_2} decreases, the points where the formation energies of these positively and negatively charged defects intersect, which is close to where charge neutrality must occur, are bound to move to higher Fermi energy.

Now, in order to discuss how the charge of the Mg_{Al}^{1-} ions is compensated and hence to explain the corundum conundrum, we introduce a graph of the concentration of each defect multiplied by the charge it contributes, versus the total magnesium concentration, Figure 2. Again we display as in Figure 1 the two separate cases of (a) ambient and (b) very low p_{O_2}. Besides all the defects, Figure 2 includes for completeness the concentrations of electrons and holes, calculated via Equations 5 and 6. Their concentrations turn out to be relatively low compared to the dominant defects, so they do not play an important part in the charge compensation of Mg.

Starting with the lowest doping levels, and looking at the ambient conditions of p_{O_2} displayed in Figure 2(a), at Mg concentrations below about 10^{-7} wt. ppm the defect concentrations deviate negligibly from those of pure Al_2O_3, in which the dominant defects are the vacancies.

TABLE II. Concentrations $[D^q]$ (in cm^{-3}) and charge concentrations $q[D^q]$ (in $e\,cm^{-3}$) of selected defects in α-Al_2O_3 containing 252 wt. ppm Mg in the experimental conditions of Ref. [6]. The share (in %) of positive charge compensation for each defect is also specified.

D^q	$[D^q]$	$q[D^q]$	share (%)
Mg_{Al}^{1-}	1.2×10^{19}	-1.2×10^{19}	—
Mg_i^{2+}	4.7×10^{18}	9.5×10^{18}	80.4
$[Mg_{Al} \cdot V_O]^{1+}$	1.6×10^{18}	1.6×10^{18}	13.4
Al_i^{3+}	1.8×10^{17}	5.5×10^{17}	4.6
V_O^{2+}	8.6×10^{16}	1.7×10^{17}	1.5
V_O^{1+}	1.8×10^{12}	1.8×10^{12}	1.5×10^{-5}
$[Mg_{Al} \cdot V_O]^0$	1.2×10^{12}	0	—
Mg_{Al}^0	4.7×10^{11}	0	—

In ambient conditions these are the Schottky quintet of V_O^{2+} and its charge-compensating V_{Al}^{3-}, in the ratio $3:2$. As the Mg concentration increases further and becomes comparable to the concentration of oxygen vacancies, the concentration of oxygen vacancies starts to increase, and the positive charge they carry tracks and compensates the charge of the Mg_{Al}^{1-} ions. But as the Mg concentra-
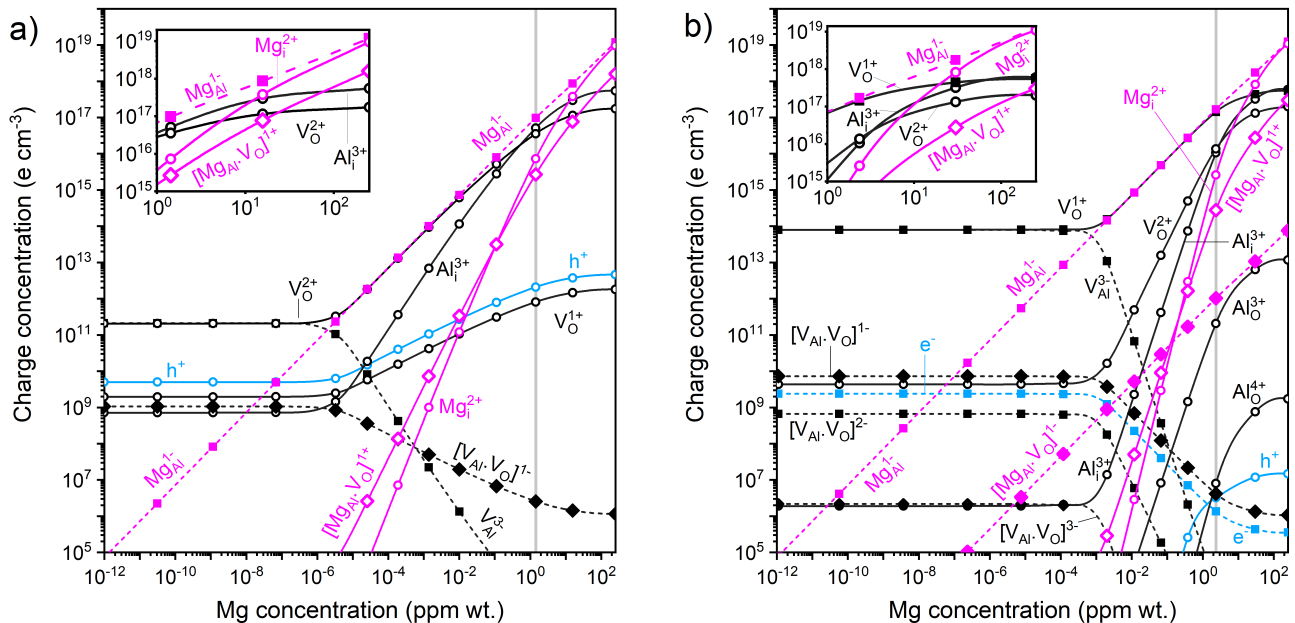
FIG. 2. Defect-charge concentrations $q[D^q]$ (in e cm^{-3}) for Mg-doped Al$_2$O$_3$ as a function of Mg doping concentrations under (a) ambient conditions ($P_{O_2} = 0.21$ atm) and (b) the reductive limit. Positively (negatively)-charged defects are represented by solid (dotted) lines. The *calculated* saturation limit for Mg (its concentration in solution if the alumina system were in equilibrium with spinel, MgAl$_2$O$_4$) is marked with a grey vertical line. The insets are magnified parts from the top-right of the diagrams, showing more clearly the dominant defects where the Mg solution is calculated to be supersaturated.

tion starts to approach 1 wt. ppm, something surprising happens, which, however, could be anticipated by studying Figure 1: the main role of compensation is taken over by aluminium interstitials, Al$_i^{3+}$. Shortly above that, the dominant compensation mechanism changes again, and the dominant compensating defect becomes Mg itself, in the form of positively charged interstitials, Mg$_i^{2+}$. At the experimental level of doping, with 252 wt. ppm of Mg, the Mg solution is mainly self-compensated by its own interstitials, and the concentration of free oxygen vacancies, V$_O^{2+}$ is two orders of magnitude less than it would have been if they were still the main compensating species. This explains the Corundum Conundrum. The details of all the defect concentrations at this Mg composition are given in Table II, where we quantify the results visible in Figure 2(a). Specifically, mobile oxygen vacancies provide only $\sim 1.5\%$ of the compensation for Mg$_{Al}^{1-}$, while $\sim 80\%$ is provided by Mg$_i^{2+}$, and a further 13% by [Mg$_{Al} \cdot V_O$]$^{1+}$ pairs, which are oxygen vacancies trapped by the Mg substitutional defect. We note that the *calculated* saturation limit of Mg is only 1.4 wt. ppm, which strongly suggests that in the dislocation loop shrinkage experiments [6], the dissolved Mg was in the supersaturated regime, since there was no evidence for precipitates of spinel in those experiments.

For completeness, we examine also the results for strongly reducing conditions displayed in Figure 2(b). The higher ε_F favours the singly charged oxygen vacan-

cies V$_O^{1+}$, and instead of the Schottky quintet seen in ambient p_{O_2} the dominant intrinsic defects at low Mg concentration are V$_O^{1+}$ and V$_{Al}^{3-}$ in the ratio 3 : 1, which we might call the Schottky quartet. At higher Mg concentrations, the compensation follows a somewhat similar pattern to the ambient oxygen case. The higher concentration of oxygen vacancies at low p_{O_2} is not matched by Mg until about 10^{-5} wt. ppm, and it then tracks and compensates the Mg$_{Al}^{-1}$ up to $\sim$ 1ppm Mg. At higher Mg concentrations the other defects take over compensation, and at 252 wt. ppm Mg the Mg$_{Al}^{-1}$ are once again compensated mainly by Mg$_i^{2+}$ interstitials.

IV. CONCLUSIONS

We have calculated the equilibrium concentrations of a range of point defects, involving one or two species of atoms, in Mg-doped α-Al$_2$O$_3$ at 1400 C, under ambient oxygen partial pressure, self-consistently determining the Fermi energy to ensure charge neutrality of the system, and with Mg contents from zero up to 252 wt. ppm With the highest Mg content, these conditions correspond to the experimental setup for the measurements of oxygen diffusion reported in ref. [2]. Our calculations make use of the 0K defect formation energies of Futazuka *et al.* ([7] and private communication). These authors obtained equilibrium defect geometries by struc-

tural relaxation using density functional theory with the PBEsol exchange-correlation functional, then calculated accurate defect formation energies and electronic densities of states corresponding for the relaxed structures using the HSE exchange-correlation functional.

The thinking behind the conundrum posed in [2] was based on the widespread theory of how the excess charge on the Mg ions, Mg_{Al}^{1-} dissolved in α-Al_2O_3 must be compensated, namely by oxygen vacancies V_O^{2+}, which are also assumed to be the agents of oxygen diffusion. The experimental concentration of Mg $(\sim 1.8 \times 10^{19}$ ions cm$^{-3})$, if it were all in the form of Mg_{Al}^{1-}, would thus require a concentration of 0.9×10^{19} oxygen vacancies per cm^{-3} for its charge compensation - according to the standard theory. Our calculations reported here have allowed several more species to enter the field, the most important of which are listed in the first column of Table II. Mg appears not only as Mg_{Al}^{1-}, but also in significant proportions of positively charged Mg interstitials, Mg_i^{2+}, and Mg -oxygen vacancy complexes, $[Mg_{Al} \cdot V_O]^{1+}$, increasing with the overall Mg content. Together with intrinsic Al interstitials, Al_i^{3+}, they all play a part in compensating the remaining negatively charged Mg_{Al}^{1-}. At the highest Mg concentration, 80% of this compensation can be described as "self-buffering" by the Mg interstitials. As a result our calculated concentration of V_O^{2+} is 0.9×10^{17} ions cm^{-3}, which is two orders of magnitude less than predicted by the standard theory. This is the solution we offer to the Corundum Conundrum.

The story is still unfinished however, since the puzzle called the Corundum Conundrum also embraces the doping of Al_2O_3 with Ti, and the compensation of Ti_{Al}^{1+} defects. We expect future work along the lines of the present paper will also reveal a more complex palette of defects, with which to resolve that case too.

ACKNOWLEDGMENTS

[1] D. S. Phillips, A. H. Heuer, and T. E. Mitchell, Precipitation in star sapphire I. Identification of the precipitate, Philos. Mag. A **42**, 385 (1980).

[2] A. H. Heuer and K. P. D. Lagerlöf, Oxygen self-diffusion in corundum (α-Al_2O_3): a conundrum, Philos. Mag. Lett. **79**, 619 (1999).

[3] A. H. Heuer, Oxygen and aluminum diffusion in α-Al_2O_3: How much do we really understand?, J. Eur. Ceram. Soc. **28**, 1495 (2008).

[4] K. Frensch, *Ab initio studies of defect concentrations and diffusion in metal oxides*, Ph.D. thesis, Imperial College London (2011).

[5] A. Tewari, U. Aschauer, and P. Bowen, Atomistic modeling of effect of Mg on oxygen vacancy diffusion in α-alumina, J. Am. Ceram. Soc. **97**, 2596 (2014).

[6] K. P. D. Lagerlof, T. E. Mitchell, and A. H. Heuer, Lattice Diffusion Kinetics in Undoped and Impurity-Doped Sapphire (α-Al_2O_3): A Dislocation Loop Annealing Study, J. Am. Ceram. Soc. **72**, 2159 (1989).

[7] T. Futazuka, R. Ishikawa, N. Shibata, and Y. Ikuhara, First-principles calculations of group IIA and group IV impurities in α-Al_2O_3, Phys. Rev. Mater. **4**, 073602 (2020).

[8] S. B. Zhang and J. E. Northrup, Chemical Potential Dependence of Defect Formation Energies in GaAs: Application to Ga Self-Diffusion, Phys. Rev. Lett. **67**, 2339 (1991).

[9] M. W. Chase Jr., NIST-JANAF Thermochemical Tables, Fourth Edition, J. Phys. Chem. Ref. Data, Monogr. 9 , 1 (1998).

[10] For legibility, we use a modified version of the Kröger-Vink notation to denote net charge states and lattice positions of point defects in α-Al_2O_3. In this notation, superscript symbols such as $''$, $^\times$, or $^{\cdots}$ in the original Kröger-Vink notation are represented instead as $^{2-}$, ^{0}, or $^{3+}$, respectively, to represent the net charge on a defect or defect cluster.

[11] G. Kresse and J. Hafner, Ab initio molecular dynamics for liquid metals, Phys. Rev. B **47**, 558(R) (1993).

[12] G. Kresse and J. Hafner, Ab initio molecular-dynamics simulation of the liquid-metal-amorphous-semiconductor transition in germanium, Phys. Rev. B **49**, 14251 (1994).

[13] G. Kresse and J. Furthmüller, Efficiency of ab-initio total energy calculations for metals and semiconductors using a plane-wave basis set, Comput. Mater. Sci. **6**, 15 (1996).

[14] G. Kresse and J. Furthmüller, Efficient iterative schemes for ab initio total-energy calculations using a plane-wave basis set, Phys. Rev. B **54**, 11169 (1996).

[15] J. P. Perdew and A. Zunger, Self-interaction correction to density-functional approximations for many-electron systems, Phys. Rev. B **23**, 5048 (1981).

[16] A. S. Brown, M. A. Spackman, and R. J. Hill, The electron distribution in corundum. A study of the utility of merging single-crystal and powder diffraction data, Acta Crystallogr. Sect. A **49**, 513 (1993).

[17] E. N. Maslen, V. A. Streltsov, N. R. Streltsova, N. Ishizawa, and Y. Satow, Synchrotron X-ray study of the electron density in α-Al_2O_3, Acta Crystallogr. Sect. B **49**, 973 (1993).

[18] Y. Wang and J. P. Perdew, Correlation hole of the spin-polarized electron gas, with exact small-wave-vector and high-density scaling, Phys. Rev. B **44**, 13298 (1991).

[19] P. Ziesche, S. Kurth, and J. P. Perdew, Density functionals from LDA to GGA, Comput. Mater. Sci. **11**, 122 (1998).

[20] J. P. Perdew, K. Burke, and M. Ernzerhof, Generalized Gradient Approximation Made Simple, Phys. Rev. Lett. **77**, 3865 (1996).

[21] J. P. Perdew, K. Burke, and M. Ernzerhof, Errata: "Generalized Gradient Approximation Made Simple" [Phys. Rev. Lett. 77, 3865 (1996)], Phys. Rev. Lett. **78**, 1396 (1997).

[22] R. H. French, Electronic Band Structure of Al_2O_3, with Comparison to AlON and AIN, J. Am. Ceram. Soc. **73**, 477 (1990).

[23] M. L. Bortz and R. H. French, Optical reflectivity measurements using a laser plasma light source, Appl. Phys. Lett. **55**, 1955 (1989).